https://doi.org/10.3311/PPci.22803
Creative Commons Attribution

Periodica Polytechnica Civil Engineering, 68(1), pp. 305–313, 2024

Assessing the Equivalent Spring Method for Modelling of Lightweight-concrete Encased Cold-formed Steel Elements in Compression

Ahmed Alabedi[1*], Péter Hegyi[1]

[1] Department of Structural Engineering, Budapest University of Technology and Economics, Műegyetem rkp. 3, 1111 Budapest, Hungary
[*] Corresponding author, e-mail: alabedi.ahmed@edu.bme.hu

Received: 13 June 2023, Accepted: 21 September 2023, Published online: 16 October 2023

Abstract

Using concrete for filling and bracing is one of the most crucial ways to improve cold-formed steel (CFS) elements' stability behavior and performance. An example is the novel building system made up by CFS encased in ultra-lightweight concrete. The numerical analysis of such structural members using solid finite elements is time-consuming, thus the need for an easy-to-use modelling technique has arisen. As a result, a simple time-efficient equivalent spring model (ESM) has been introduced as a viable method for properly analyzing complex structural behavior in numerous cases, replacing the concrete solid with one-directional springs applying the Winkler foundation. This study aims to examine the validity and limitations of the ESM by comparing it to 3D solid model (SMOD) results for internal plate elements. The analysis results indicate that the ESM could provide accurate results in the *b*/*t* range of 100 or less for a wide range of PAC modulus (50–250 MPa) with an error of less than 5%; hence, using spring in modelling PAC within these limits is deemed acceptable. Nevertheless, for larger *b*/*t* values up to 175, doubled the calculated spring stiffness is highly recommended. In addition, the results reveal that the applicability of ESM is limited for *b*/*t* above 175; the model fails to predict the ultimate failure load, and the failure mode. Finally, this study ends by recommending one equation for calculating equivalent foundation spring stiffness for internal components that ensure optimal performance of the ESM analysis.

Keywords

plate buckling, ultimate load bearing capacity, numerical analysis, simplified model, equivalent spring model

1 Introduction

1.1 Advancement in cold-formed steel

Cold-formed steel (CFS) constructions have become increasingly common in low- and mid-rise buildings as more efficient alternatives to hot-rolled steel and reinforced concrete. These cost-effective structures, characterized by substantial advantages, such as their light weight, speed of production, ease of manufacturing, and no need for formwork, helped spread of these elements. Hence, CFS elements have become widely utilized as major load-bearing constructions such as pallet racks, industrial blinding, and residential houses [1, 2].

As load-bearing components, CFS elements are characterized by their stability failure mechanism (i.e., local, distortional, or global buckling); therefore, numerous studies were conducted in this field using intensive experiments and analytical approaches using concrete for filling and bracing is one of the possible ways to improve the behavior and performance of CFS elements.

Research papers [3, 4] improved the CFS by bracing the corrugated steel sheet with various infill materials such as lightweight, plain, and fiber-reinforced foamed concrete. Their findings demonstrated the importance of the infill material, demonstrating how lightweight foamed concrete enhances structural response, leading to an innovative structural system with a sufficient load-carrying capacity that may be utilized for low-rise structures. Likewise, a novel investigation path was carried out by Hegyi et al. [5, 6], who intended to improve the stability of CFS members utilizing polystyrene aggregate concrete (PAC) as encasing material. Intensive experiments were conducted on CFS flexural [2], compression [5] elements and shear panels [1, 6]. The braced CFS experiments demonstrated that PAC significantly impacts the stability of CFS, hence increasing its load-bearing capacity.

Cite this article as: Alabedi, A., Hegyi, P. "Assessing the Equivalent Spring Method for Modelling of Lightweight-concrete Encased Cold-formed Steel Elements in Compression", Periodica Polytechnica Civil Engineering, 68(1), pp. 305–313, 2024. https://doi.org/10.3311/PPci.22803

On the other hand, CFS structures and components have been numerically studied using finite element technique, producing satisfactory results with reasonable computational time. Cold-formed steel purlins and the supporting structure connection were numerically analyzed by Pařenica et al. [7]. Majdi et al. [8] created a model for characterizing the bond-slip behavior of galvanized CFS components embedded in concrete. Furthermore, numerous research addressed modelling thin-walled steel built-up members [9–12].

The numerical analysis of PAC-encased CFS structural members using solid finite elements is time-consuming, thus the need for an easy-to-use modelling technique has arisen. Eid et al. [13] introduced a simplified finite element model for analyzing such elements in which the encasing material (PAC) was considered fully elastic, and its volume was substituted by equivalent springs representing Winkler-type foundation. A modelling framework for structural members was developed where the equivalent spring stiffness was defined based on the critical buckling stress using the approximated equation in [14]. The modelling framework was calibrated to experimental data of compressed C-section members found in [5]. The modelling framework showed acceptable results, but it also has its limitations.

1.2 Aims

The purpose of the current study is to have a deeper understanding of the equivalent spring model (ESM) of Eid et al. [13] and to compare its performance to a detailed 3-D solid FE model (later on referred as SMOD). The ESM was developed for and verified against C-sections. We aim to examine the validity and limitations of this model on single plates having four simply supported edges. Comparison will be made on the critical and ultimate load levels, ESM coefficients will be assessed and improvements will be proposed. After additional research work on outstand plate members the final aim is to make the ESM method useful for different cross-sections, making it a universal tool for calculating the resistance of elastic material encased CFS cross-sections.

2 Development of numerical model

For the C-section in Fig. 1(a), the web and flange are internal elements. Such type of element can be represented as a plate with simply supported edges subjected to uniaxial compression, Fig. 1(b). Similarly, the stiffeners in Fig. 1(c) are outstand elements, modelled as simply supported plates with one free edge. In this study, two FE models of internal plates encased in elastic material will be built using ANSYS software [15] following the modelling guidelines described in EC3-1-5. One FE model used the ESM method, and the other (SMOD) solid elements to represent the elastic medium.

There is a significant mechanical difference between the SMOD and ESM models. The SMOD utilizes a 3D solid with shear stress effects; hence, the "vertical" stabilizing stress of the foundation depends on the overall plate displacement shape. In contrast, ESM uses a Winkler-type foundation, connecting foundation stress solely to plate displacement at a given point.

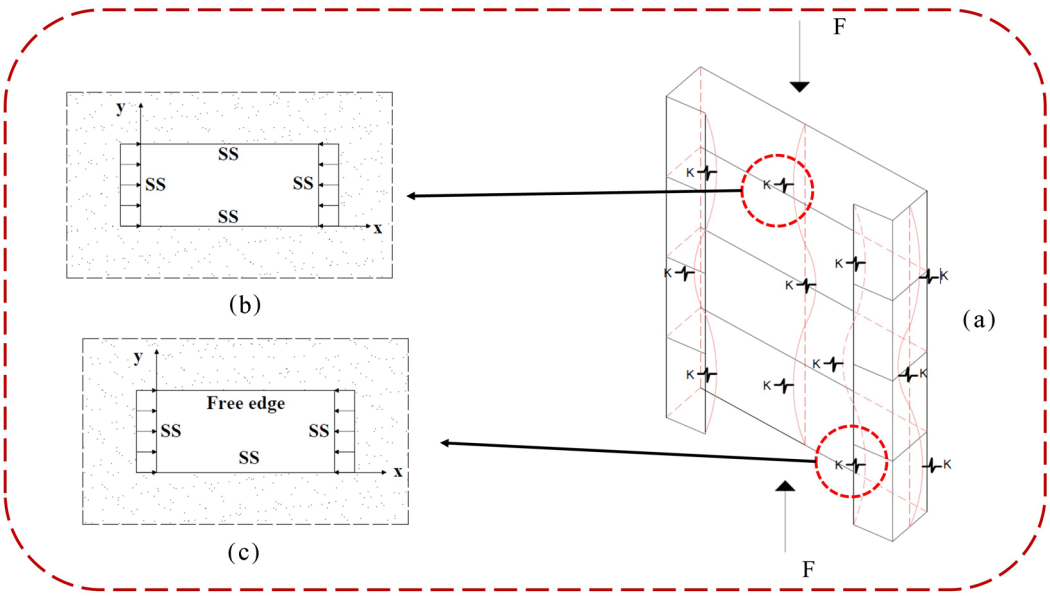

Fig. 1 (a) Braced CFS section (b) internal plate (c) outstand plate

To examine the validity and limitations of the ESM method for internal elements, a wide range of cases must be covered; thus, the parameters detailed in Table 1 were used in this study: b/t, E_c, and mesh size (A), where b and t are the width and thickness of plate, respectively, and E_c is the Young's modulus of the elastic medium. The two braced models are further detailed in Sections 2.1 and 2.2.

2.1 SMOD FEM development

The SMOD FEM plate geometry was modelled using 4-node shell elements (SHELL181) with a bilinear stress-deformation curve having isotropic hardening. The thickness was adjusted to 1 mm, and the width of the plate was changed in accordance with Table 1. The plate length (l_x) was set to be six times the estimated buckling length to achieve long plate behavior [14]. To eliminate rigid body motion, all plate edges were restricted in the out-of-plane Z-direction, with one central node fixed in the cross Y-direction. The elastic material was modelled using the 8-node solid element SOLID185. The dimensions were adjusted to maintain the half-space-like behavior of the solid following the recommendation in [14] (see Fig. 2).

To optimize the connection between solid and plate, the exact same pattern of finite elements was utilized in the interface zones. In the side areas of the solid, a 15-times bigger finite element size was used to minimize calculation demand. The material behavior was considered to be linear elastic with no cracking or crushing, as these phenomena affect only the post-failure behavior of plates. Both tension and compression were transferred between the two materials since the steel plate is connected to the elastic material from only one side (whereas it is usually encased from both sides in reality). By using this modelling technique, the real behavior could be maintained.

Table 1 Parameter range of the numerical investigation

Parameter	Range
Plate slenderness (b/t)	50–250
Yield strength of steel (f_y)	180–380 MPa
Elastic modulus (E_c)	50–250 MPa
Mesh size (A)	(5 × 5)–(20 × 20) mm^2

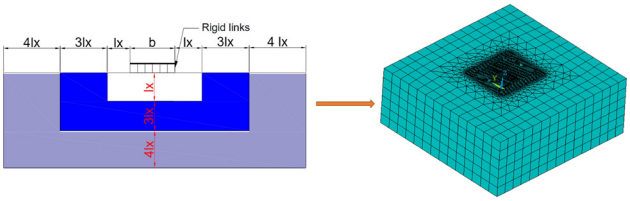

Fig. 2 SMOD FEM geometry

The plate and the elastic foundation were connected by a 1D rigid link (COMBIN14) acting perpendicular to the surface. The rigid link only transmitted movements perpendicular to the plate (i.e., no in-plane motion generated contact forces). The nonlinear analysis was performed incorporating material nonlinearity and geometrical imperfections (GMNIA). Imperfection was defined as the first eigenshape of the model and scaled by $b/200$ amplitude, following the recommendation of Eurocode.

2.2 ESM FEM development

This model is characterized by the normal stiffness of the foundation springs. The plate was modelled using SHELL181 element as described before, with the elastic half-space replaced by linear unidirectional springs using the COMBIN40 element. Each node of the plate was connected to a spring in the Z-direction (see Fig. 3).

Spring stiffness was calculated using Eq. (1) [13], where a, b, c, d, e and f are constants according to Table 2. Plate length, width and thickness was set as described before. Similar to Section 2.1 nonlinear analysis was performed, incorporating material nonlinearity and geometrical imperfections (GMNIA).

$$K = a\left[\frac{N}{mm}\right] + b\left[\frac{N}{mm^3}\right]A + c[mm]E_c + d\left[\frac{N}{mm^5}\right]A^2 + e\left[\frac{1}{mm}\right]AE_c + f\left[\frac{mm^3}{N}\right]E_c^2 \quad (1)$$

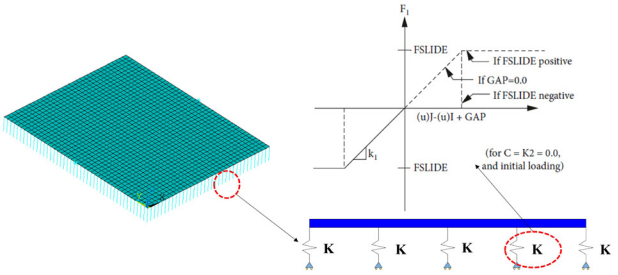

Fig. 3 ESM FEM geometry

Table 2 Coefficients of Eq. (1) of internal compressed plates [13]

b/t	a [N/mm]	b [N/mm^3]	c [mm]	d [N/mm^5]	e [1/mm]	f [mm^3/N]
50	-203.2	5.231	1.942	-0.0236	0.02615	0.001267
100	-228.7	3.028	2.628	-0.00629	0.01938	0.0015
175	-197.3	3.147	2.002	-0.0068	0.02156	0.003725
250	-262.9	3.668	2.82	-0.00802	0.02174	0.001072

2.3 Verification of unbraced numerical models

To ensure the reliability of the numerical models, the unbraced plates' performance was assessed. The results of the unbraced models (i.e., when E_c or K was set to zero) were compared to analytical values, as shown in Fig. 4. Comparison was made using the critical stress (see Fig. 4(a)), and the normalized ultimate strength of the plate (i.e., $\rho = N_{u,\mathrm{FEM}}/btf_y$)), too (see Fig. 4(b)).

The FE outcomes showed that the model could predict the expected ultimate load effectively with a maximum relative difference of 4.9%. The nonlinear performance of the finite element model was adequate in accordance with those reported in the literature database [16–18].

2.4 Assessment of braced numerical models

The performance of the ESM FE model was first assessed using the critical stresses. The basis of assessment was the critical stress determined using Eq. (2), which is an approximate formula fitted to analytical results [14]. According to Eq. (1), the equivalent spring stiffness is a function of the element size; therefore, a mesh sensitivity study was carried out to find the plate's optimum mesh size on the investigated parameter range. Consequently, it has been found that (6 × 6) mm element size gives the most accurate estimation in the parameter range with a maximum difference of 9 %. Fig. 5(a) presents the error of the ESM against the plate b/t ratio. It can be noticed that the maximum discrepancy was 5% for small b/t values but increased to 9% for higher ones. Generally, the higher the foundation modulus, the higher the error. The trend of results indicates that the calculated stiffness based on Eq. (1) is higher than needed. Fig. 5(b) further illustrates this error trend by plotting the calculated critical buckling stress of Eq. (2) against the plate b/t ratio with continuous lines, considering different elastic moduli. The discrete data points in the graph correspond to values obtained using the ESM. The observed 9% error in critical stress results in 3% overestimation of ultimate load bearing capacity if the Winter-curve of the Eurocode standard is used.

$$\sigma_{cr,p} = 4\frac{\pi^2 E_s}{12\left(1-\nu_s^2\right)(b/t)^2} - \frac{480\,MPa}{b/t} + 2.35E_c + \sqrt{E_c 3025\,MPa} \tag{2}$$

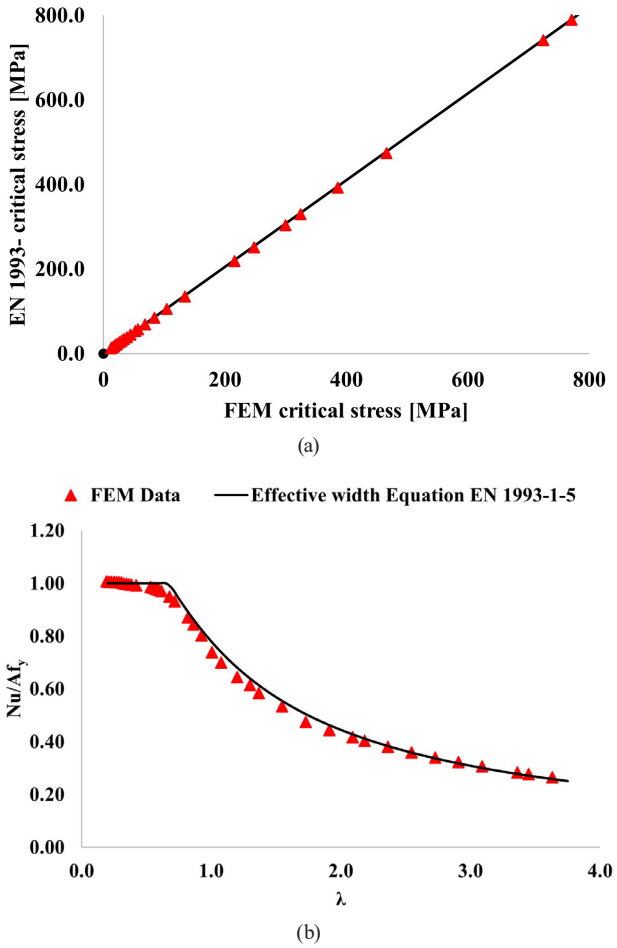

Fig. 4 Verification of unbraced FE model (a) critical stress, (b) normalized ultimate strength

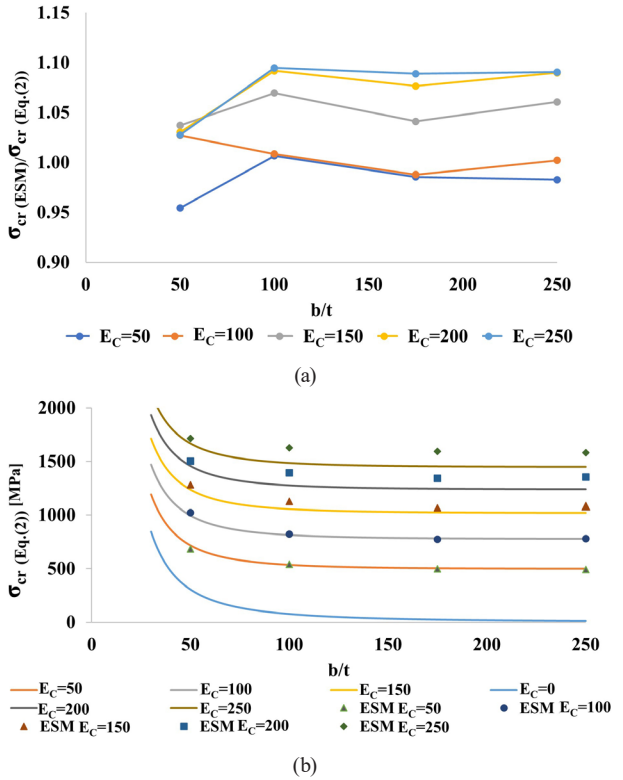

Fig. 5 Verification of ESM, (a) error – b/t relation, (b) Eq. (2) computed stress values as function of b/t considering different elastic moduli versus ESM critical stress results

Similarly, the results of SMOD critical stress were compared to the values of Eq. (2). In the verification procedure, the same 6 × 6 mm mesh size was maintained for comparison purposes. Results can be seen in Fig. 6. In the applied parameter range, the highest difference of SMOD results is 10%, the method underestimates Eq. (2). Fig. 6(a) compares the SMOD critical stress and the computed stresses from Eq. (2). For smaller *b*/*t* values (*b*/*t* = 50), the SMOD results show accurate agreement with the calculated values. As the *b*/*t* ratio increases, the error gradually increases, with a discrepancy of 10% observed when the *b*/*t* ratio reaches 250.

SMOD results show different error trends as ESM results. The reason is the different mechanical formulation of the two approaches. This relationship is also illustrated in Fig. 6(b), where the computed critical buckling stress obtained from Eq. (2) is plotted against the *b*/*t* ratio as continuous lines for different foundation elastic moduli, and SMOD results are indicated as data points in the plot. The observed 10% error in critical stress results in 3–4% underestimation of ultimate load bearing capacity if the Winter-curve of the Eurocode standard is used.

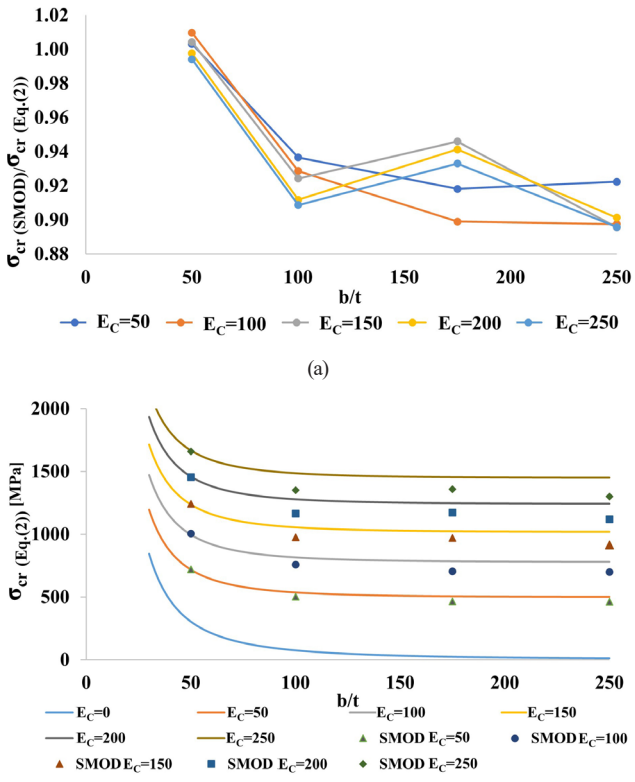

Fig. 6 Verification of SMOD (a) error – *b*/*t* relation, (b) Eq. (2) computed stress values as function of *b*/*t* for different elastic moduli versus SMOD critical stress results

3 Evaluation of ESM for ultimate strength

3.1 Original procedure

The performance of ESM and SMOD were similar thus it was considered appropriate to compare the ultimate strength results of the models to each other. The analysis results showed that the ESM could match the SMOD model for *b*/*t* values lower or equal to 100 with a maximum average difference of 3%. For larger *b*/*t* ratios, the results revealed a significant impact of plate yield strength on the difference between the two models; a higher difference was observed for higher f_y values.

Fig. 7 demonstrates the error (N_{ESM}/N_{SMOD}) as a function of *b*/*t* for different E_c and f_y.

Similarly, regarding load-displacement curves and failure mechanisms, the ESM and SMOD coincide quite well. Fig. 8 illustrates the load-displacement curves for two different plates. As a result, ESM could precisely predict the ultimate load for a wide range of concrete modulus (50–250 MPa) for *b*/*t* less or equal to 100, and hence, using

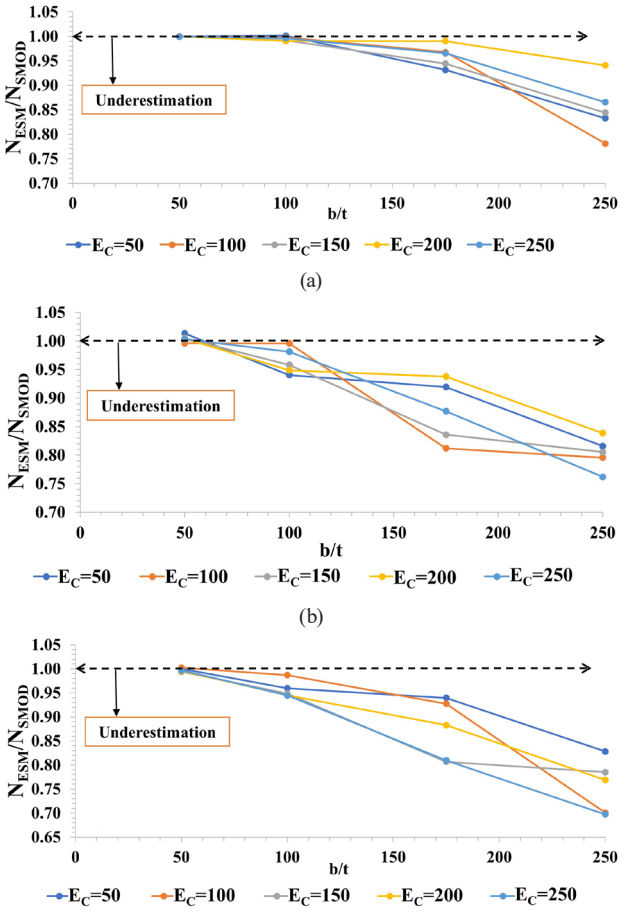

Fig. 7 ESM error as function of b/t: (a) f_y = 180 MPa, (b) f_y = 280 MPa, (c) f_y = 380 MPa

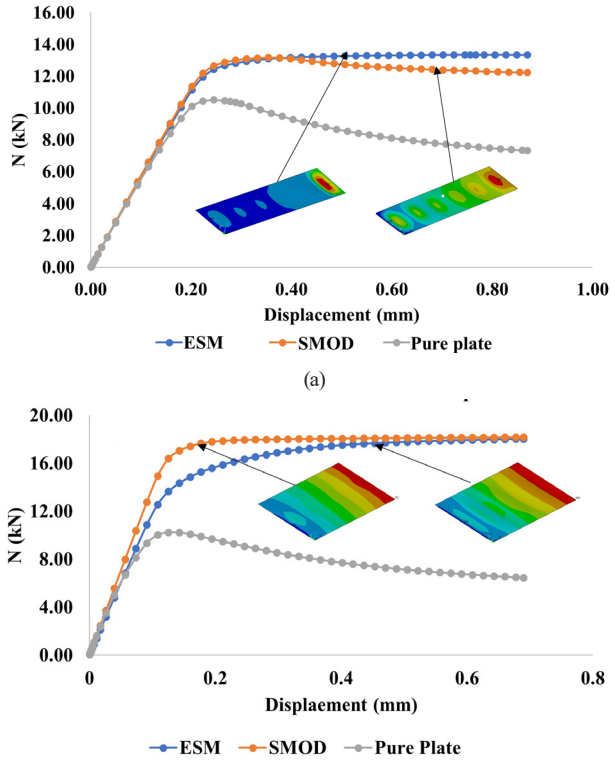

Fig. 8 Load-displacement curves: (a) b/t = 50, E_c = 50, f_y = 280 MPa, (b) b/t = 100, E_c = 150, f_y = 180 MPa

spring in modelling PAC within these limits is deemed favorable. The results also indicate that the ESM should be recalibrated for large b/t ratio (i.e., 175, 250) to widen the range of accurate use.

3.2 Recalibration of spring stiffness

Modifying the stiffness of the foundation springs could significantly affect the performance of the ESM. Given that for small b/t Eq. (1) demonstrated good agreement with the SMOD, the entire analysis process was redone for every b/t value by using constants corresponding to b/t = 50 in Eq. (1) for calculating spring stiffness.

The analysis showed that incorporating new K values does not have significant effect on the ESM performance for lower-strength plates, see Fig. 9(a). Fig. 10 demonstrates load-displacement curves and failure modes of b/t = 175 for E_c = 250 and f_y = 180 MPa with a 1% difference using b/t = 50 constants.

For higher plate strengths (i.e., 280 MPa and beyond), the recalibration slightly affected the performance of ESM. This led to a moderate improvement in reducing the overall average error from 13% to 10% for b/t 175 and from 20% to 17% for b/t 250 with f_y = 280 MPa (see Fig. 9(b)). Similar behavior can be noticed for the highest investigated yield strength by comparing Fig. 9(c) to

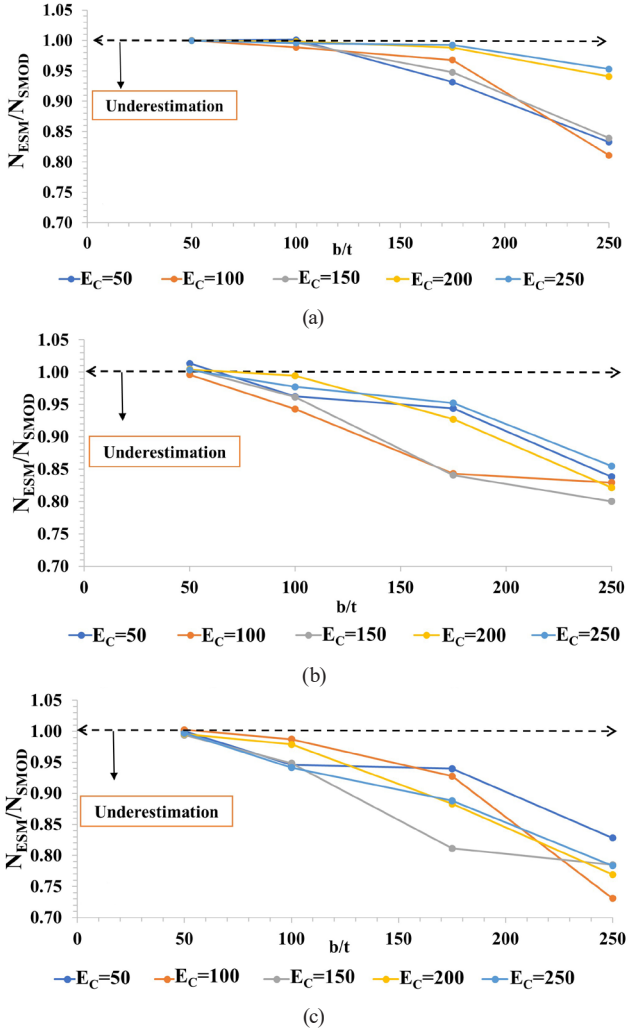

Fig. 9 ESM error using constants corresponding to b/t = 50 in Eq. (1) as function of b/t (a) f_y = 180 MPa, (b) f_y = 280 MPa, (c) f_y = 380 MPa

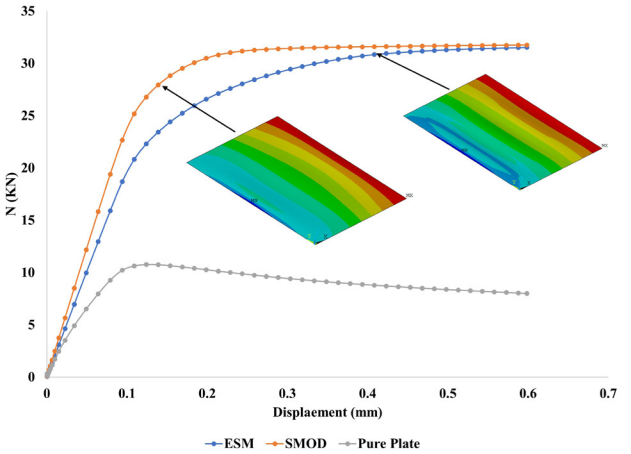

Fig. 10 Load-displacement curves b/t = 175, Ec = 250, f_y = 180 MPa ESM spring stiffness calculated based on b/t = 50 constants

Fig. 7(c). The results also indicated that the ESM still had limitations for large b/t values (i.e., 175 and higher), specifically for high plate strength; thus, further enhancement is needed.

A parametric study was carried out on the equivalent spring stiffness by implementing different values up to 35000 N/mm for large *b*/*t* ratios (i.e., 175, 250). The conducted study showed that for f_y = 280 MPa and beyond doubling the calculated foundation stiffness (using constants corresponding to *b*/*t* = 50 in Eq. (1)) leads to a considerable improvement in the performance of the ESM for *b*/*t* equal to 175. This enhancement reduces the maximum difference between the two models to 6%, particularly in the mean values of the elastic modulus range (see Fig. 11(a) and (b)).

On the other hand, the conducted study also revealed that this increment of K does not affect the ESM performance for even higher *b*/*t* ratios. In the case of *b*/*t* = 250 (see Fig. 12(a)), the results show that significant additional increment in the foundation stiffness is needed to increase the ultimate strength of the plate which simultaneously affect the mode of failure as well. Increasing the spring stiffness up to high values increases the number of half-waves, resulting in different failure shapes [14] (see Fig. 12(b)).

In summary, the recalibration process indicated that incorporating the constant *b*/*t* = 50 value in Eq. (1) improved the performance of the ESM; hence, Eq. (3) can be used efficiently to represent the effect of elastic foundation. For higher strength plates (280 MPa and beyond), the recalibration process revealed that doubling the calculated

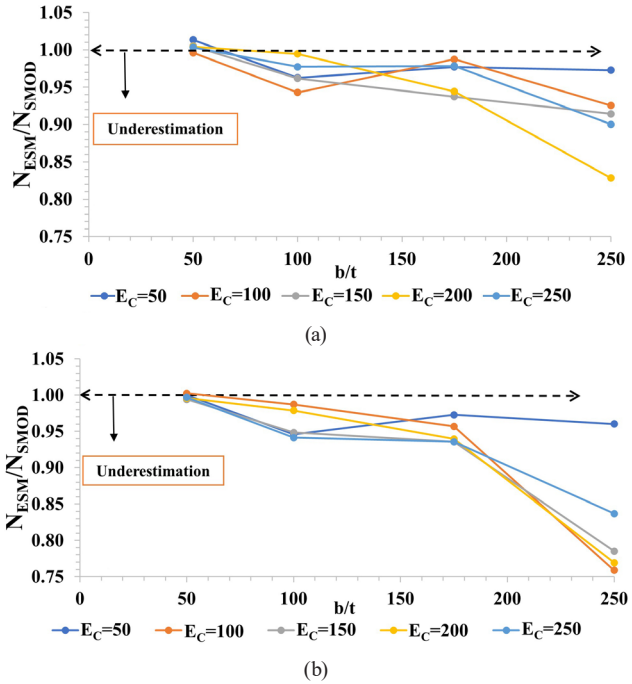

Fig. 11 ESM error for calibrated spring stiffness as function of *b*/*t*: (a) f_y = 280 MPa, (b) f_y = 380 MPa

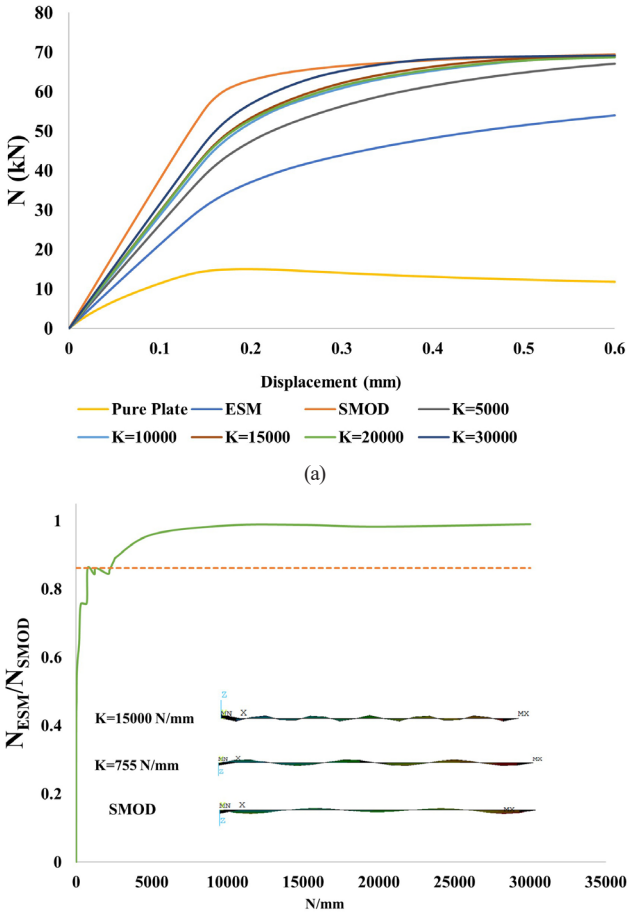

Fig. 12 (a) Load-displacement curve *b*/*t* = 250 compression using different *K* value, (b) spring stiffness sensitivity study

spring stiffness of Eq. (3) can reduce the error for high *b*/*t* up to 175; hence, using modified values deemed favorable. In contrast, for even higher *b*/*t* values, the conducted study showed that using the ESM is unfavorable. In the range of the investigated parameters, the ESM failed to provide results consistent with the SMOD. For such *b*/*t* ratios, increasing the equivalent spring stiffness is not appropriate since it can provide the required ultimate load only by significantly altering the failure mode of the plate.

$$K = -203.2 + 5.231A + 1.942E_c - 0.02615A^2 + 0.02615AE_c + 0.001267E_c^2 \quad (3)$$

4 Conclusions

This paper discusses the equivalent spring method (ESM), which is a simplified technique to model the effect of elastic bracing material in encased cold-formed steel sections. A GMNIA parametric study was conducted on a wide range of internal plate elements regarding the critical stress, ultimate failure load, load-displacement curve and

failure mode. The results of the ESM model were compared to 3D solid FE model results (SMOD) to analyze the performance of the simplified method. Some conclusions based on the results can be given as follows:

1. It was shown that the ESM provides accurate ultimate load-bearing capacity, failure shape and load-displacement curve for internal plates in the *b*/*t* range of 100 or less for a wide range of PAC modulus (50–250 MPa) with an error of less than 5%.
2. A recalibration process was carried out to improve the performance of the ESM and reduce the overall error using constants corresponding to *b*/*t* = 50 in Eq. (1) resulting in Eq. (3) for calculating the equivalent spring stiffness.
3. For large *b*/*t* ratios (i.e., 175), the recalibration process revealed that Eq. (3) could effectively represent the effect of the elastic foundation if spring stiffness values are doubled.
4. For even higher *b*/*t* values (i.e., over 175) of internal plates, the study showed that using the ESM is unfavorable; the ESM fails to provide results consistent with the SMOD.

Using the proposed equivalent spring method, the axial load-bearing capacity calculation of sections encased in elastic material can be carried out using less computational effort and for different cross-section shapes (such as box-section). The method can be extended for outstand plates and even consider the resistance against bending moment and bending-axial load interaction to widen the application range of the method.

Acknowledgment

This research project is part of a doctoral program supported by the Stipendium Hungaricum Scholarship scheme, and founded by the Hungarian Government, Tempus Public Foundation.

References

[1] Hegyi, P., Dunai, L. "Experimental Investigation of Thin-walled Column-end Joints Encased in Ultra-lightweight Concrete", Periodica Polytechnica Civil Engineering, 61(4), pp. 951–957, 2017. https://doi.org/10.3311/PPci.10041

[2] Hegyi, P., Dunai, L. "Experimental study on ultra-lightweight-concrete encased cold-formed steel structures Part I: Stability behaviour of elements subjected to bending", Thin-Walled Structures, 101, pp. 75–84, 2016. https://doi.org/10.1016/j.tws.2016.01.004

[3] Othuman Mydin, M. A., Wang, Y. C. "Structural performance of lightweight steel-foamed concrete–steel composite walling system under compression", Thin-Walled Structures, 49(1), pp. 66–76, 2011. https://doi.org/10.1016/j.tws.2010.08.007

[4] Flores-Johnson, E. A., Li, Q. M. "Structural behaviour of composite sandwich panels with plain and fibre-reinforced foamed concrete cores and corrugated steel faces", Composite Structures, 94(5), pp. 1555–1563, 2012. https://doi.org/10.1016/j.compstruct.2011.12.017

[5] Hegyi, P., Dunai, L. "Experimental investigations on ultra-lightweight-concrete encased cold-formed steel structures: Part II: Stability behaviour of elements subjected to compression", Thin-Walled Structures, 101, pp. 100–108, 2016. https://doi.org/10.1016/j.tws.2016.01.003

[6] Hegyi, P., Horváth, L., Dunai, L., Ghazi, A. A. M. "Experimental Investigation of Shear Effects in Ultra-Lightweight Concrete Encased CFS Structural Members", ce/papers, 5(4), pp. 143–150, 2022. https://doi.org/10.1002/cepa.1739

[7] Pařenica, P., Rosmanit, M., Flodr, J. "Numerical Modelling of Thin-walled Purlins Connection to the Supporting Structure", Procedia Engineering, 190, pp. 186–192, 2017. https://doi.org/10.1016/j.proeng.2017.05.325

[8] Majdi, Y., Hsu, C.-T. T., Punurai, S. "Local bond–slip behavior between cold-formed metal and concrete", Engineering Structures, 69, pp. 271–284, 2014. https://doi.org/10.1016/j.engstruct.2014.03.025

[9] Anbarasu, M. "Simulation of flexural behaviour and design of cold-formed steel closed built-up beams composed of two sigma sections for local buckling", Engineering Structures, 191, pp. 549–562, 2019. https://doi.org/10.1016/j.engstruct.2019.04.093

[10] Li, Y.-L., Li, Y.-Q., Shen, Z.-Y. "Investigation on flexural strength of cold-formed thin-walled steel beams with built-up box section", Thin-Walled Structures, 107, pp. 66–79, 2016. https://doi.org/10.1016/j.tws.2016.05.026

[11] Roy, K., Ting, T. C. H., Lau, H. H., Lim, J. B. P. "Nonlinear behaviour of back-to-back gapped built-up cold-formed steel channel sections under compression", Journal of Constructional Steel Research, 147, pp. 257–276, 2018. https://doi.org/10.1016/j.jcsr.2018.04.007

[12] Selvaraj, S., Madhavan, M. "Structural Design of Cold-formed Steel face-to-face Connected Built-up beams using Direct Strength Method", Journal of Constructional Steel Research, 160, pp. 613–628, 2019. https://doi.org/10.1016/j.jcsr.2019.05.053

[13] Eid, N., Joó, A. L. "Simplified Numerical Model Development for Advanced Design of Lightweight-Concrete Encased Cold-Formed Steel Compressed Elements", Advances in Civil Engineering, 2022, 1207885, 2022. https://doi.org/10.1155/2022/1207885

[14] Hegyi, P., Dunai, L. "07.18: Cold-formed C-sections encased in ultra-lightweight concrete: Development of a Eurocode-based design method", ce/papers, 1(2–3), pp. 1647–1656, 2017. https://doi.org/10.1002/cepa.208

[15] Ansys® Academic Research "R2, help system, structural analysis, Guide", 2022.

[16] Wang, J., Afshan, S., Schillo, N., Theofanous, M., Feldmann, M., Gardner, L. "Material properties and compressive local buckling response of high strength steel square and rectangular hollow sections", Engineering Structures, 130, pp. 297–315, 2017. https://doi.org/10.1016/j.engstruct.2016.10.023

[17] Rasmussen, K. J. R., Hancock, G. J. "Plate slenderness limits for high strength steel sections", Journal of Constructional Steel Research, 23(1–3), pp. 73–96, 1992. https://doi.org/10.1016/0143-974X(92)90037-F

[18] Shi, G., Zhou, W., Bai, Y., Lin, C. "Local buckling of 460 MPa high strength steel welded section stub columns under axial compression", Journal of Constructional Steel Research, 100, pp. 60–70, 2014. https://doi.org/10.1016/j.jcsr.2014.04.027